

## Soot Formation in a Shock Tube under Elevated Pressure Conditions

H. KELLERER, A. MÜLLER, H.-J. BAUER and S. WITTIG *Institut für Thermische Strömungsmaschinen Universität Karlsruhe Kaiserstr. 12 76128 Karlsruhe Germany*

(Received March 1, 1996)

**Abstract**—High pressure soot formation from methane, ethylene, acetylene, propane and *n*-heptane was studied at rich burning conditions applying the shock tube technique. Pressure behind reflected shock was varied between 15 and 100 bar. Time resolved measurements of soot particle diameter and number density were carried out using an extinction-scattering technique at 488 nm. It could be shown that soot formation at high pressures is characterized by particle diameters below 30 nm that decrease with pressure. The corresponding high particle number densities in the range of  $N \approx 10^{12} - 10^{13} \text{ 1/cm}^3$  turned out to be considerably higher than at atmospheric conditions. This behavior has to be attributed to reduced coagulation coefficients in the transition regime between free molecular and continuum flow. It was found that an increase in carbon concentration has a strong promoting influence on soot volume fraction. Total pressure, however, does significantly enhance soot yield at pressures up to 30 bar and loses its dominance at higher pressures.

**Key words:** Soot, pressure, shock tube, environmental studies.

### INTRODUCTION

One of the limits of high-pressure combustion in combustion chambers for engine applications is the problem of high radiative heat transfer as a result of the soot loading of the flame. The pressure in these devices ranges from 15 to 45 bar for advanced aero engines and even higher pressures for Diesel-engines. Therefore, understanding of mechanisms of soot formation at elevated pressures is of growing importance in the design of advanced combustion chambers.

Experimental studies of sooting processes, to date, have focused primarily on low-pressure or atmospheric conditions. As only few experiments at high pressure conditions were carried out, soot formation at high pressures is still an insufficiently understood subject. A survey of pressure effects on soot formation is given by Wagner (1987). Fundamental investigations on the influence of pressure on soot formation have been carried out in shock tubes for rich oxidation by Müller and Wittig (1994). They could demonstrate the methane soot yields rises proportional to the fuel partial pressure, whereas total pressure has a strong promoting influence at 30 bar that diminishes towards higher pressures. Extensive measurements of shock tube pyrolysis by Bauerle *et al.* (1994) indicated that the effect of pressure on soot formation is strongly dependent on the hydrocarbon fuel used. Whereas almost no influence of total pressure on *n*-hexane soot yields were found, ethylene soot yields resulted to scale with pressure and benzene soot yields diminished as total pressure was increased. Parker *et al.* (1989) investigated toluene pyrolysis from 10 to 30 bar. They could show that higher carbon concentration leads to a strong increase of soot yield. However, enhanced total pressure showed no influence on soot yield but

shifted the temperature of maximum soot yield towards lower temperatures. Premixed flames at elevated pressures were studied to a great extent by Böhm *et al.* (1992). Their analysis for  $C_2H_4$ -flames showed that soot volume fraction  $f_v$  rises proportional to  $p$  for pressures higher than 10 bar.

For the understanding of high pressure soot formation information on soot volume fraction with respect to  $T, p$  and  $[C]$  is of major interest. However, as coagulation as well as surface growth reactions depend on pressure, more detailed insight can be gained by separately obtain particle diameter and number density. Therefore, the aim of the study presented was to achieve time-resolved measurements of these properties. Additionally, the influence of total pressure and carbon concentration on soot formation of the fuels under investigation was to be studied.

## EXPERIMENTAL

The experiments were carried out in a conventional shock tube (Fig. 1) which was essentially that described by Wittig *et al.* (1989). It is 4950 mm in total length with a driven section of 2970 mm. The inner diameter is 31.4 mm. The shock tube was equipped with three piezoelectric pressure transducers to measure the shock speed and determine the pressure in the measurement plane. Applying the ideal gas law and equation of state the thermodynamic state in the measurement plane could be derived. Shocks were started by disruption of mylar diaphragms. Optical investigations were carried out behind the reflected shock, 10 mm in front of the end wall. In the plane of measurement three windows were mounted to allow optical access for extinction and scattering at  $90^\circ$ . Gas mixtures were prepared manometrically using gases of high purity. Mixing was carried out by convection and magnetic stirring.

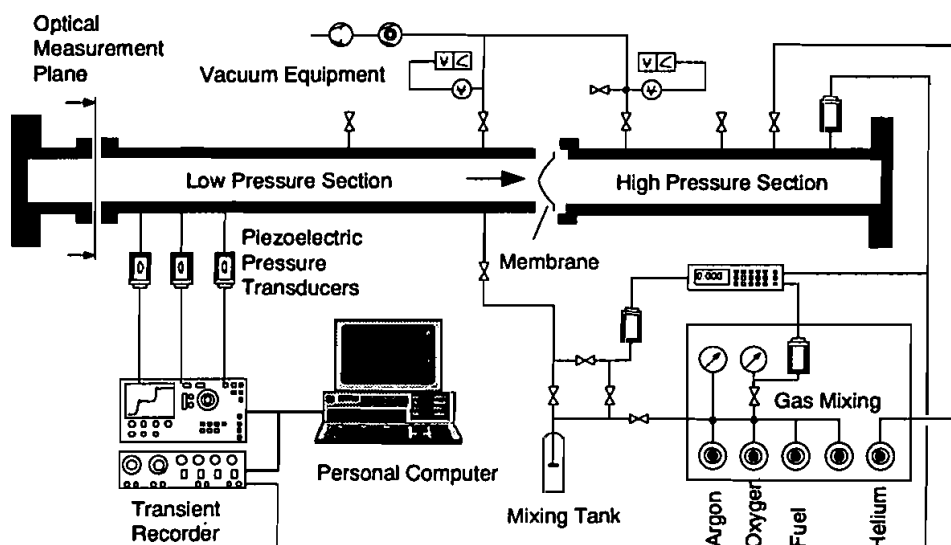


FIGURE 1 Shock tube facility for enhanced pressure soot formation experiments.

The shock tube was cleaned and evacuated before each run. The applied pressure ranged from 15 to 100 bar, temperature from 1600 to 2100 K and carbon concentration was varied between 3 and 14 mol/m<sup>3</sup>. Hydrocarbons under investigation were methane, acetylene, ethylene, propane and n-heptane. The equivalence ratios studied ranged from 3 to 5 with gas mixtures being highly diluted in argon.

## OPTICAL SETUP

A scattering-extinction method was applied to follow soot particle growth, as multi-wavelength-extinction techniques proved not to give reliable results in shock tube soot formation (Kellerer *et al.* 1995). For the scattering measurements a c.w. 3 Watt Ar<sup>+</sup>-laser operated at 488 nm was used as light source. Scattered light was detected at a scattering angle of 90°. To discriminate scattering against emission, a motor powered mechanical beam chopper (40 kHz) was used. Laser light polarization was rotated by a  $\lambda/2$ -plate to allow VV-scattering. The scattered light was filtered by a polarizer and a narrow banded interference filter ( $488 \pm 0.45$  nm) before being focused on a pinhole in front of a photo-multiplier tube. Adjustment of the optics was performed by means of a beam-splitter cube and a thin piece of wire that were placed in the measurement volume. The scattering signal was corrected for vacuum scattering caused by reflections on windows and the shock tube wall. The detection of the transmitted light was done by means of Si-photodiodes. The scattering-extinction system was calibrated by scattering from argon atoms of known scattering cross section of  $7.7 \cdot 10^{-28}$  cm<sup>2</sup>sr<sup>-1</sup> (Rudder and Bach 1968). A log-normal particle size distribution with  $\sigma_g = 0.2$  was chosen, based on results achieved by TEM primary particle analysis. This is in accordance with studies by Bauerle *et al.* (1994). The wavelength dependent values for the real and imaginary part of the refractive index  $m$  were calculated using the dispersion model with constants suggested by Lee and Tien (1981).

Direct determination of the particle diameter is only possible for monodisperse particles in the Rayleigh regime. Then scattering and absorption coefficients have to be evaluated that are given by:

$$Q_{VV} = \frac{\pi^4}{4\lambda^4} \left| \frac{m^2 - 1}{m^2 + 2} \right|^2 N d^6 \quad (1)$$

$$K_{ABS} = -\frac{\pi^2}{\lambda} \text{Im} \left\{ \frac{m^2 - 1}{m^2 + 2} \right\} N d^3 \quad (2)$$

where  $d$  and  $N$  are particle diameter and number density. In accordance with the presumed size distribution scattering and extinction coefficients were determined by Mie calculation as:

$$Q_{VV} = \frac{\lambda^2}{4\pi^2} N \int_0^\infty p(d) i_\perp dd \quad (3)$$

$$K_{EXT} = N \int_0^\infty p(d) C_{ext} dd \quad (4)$$

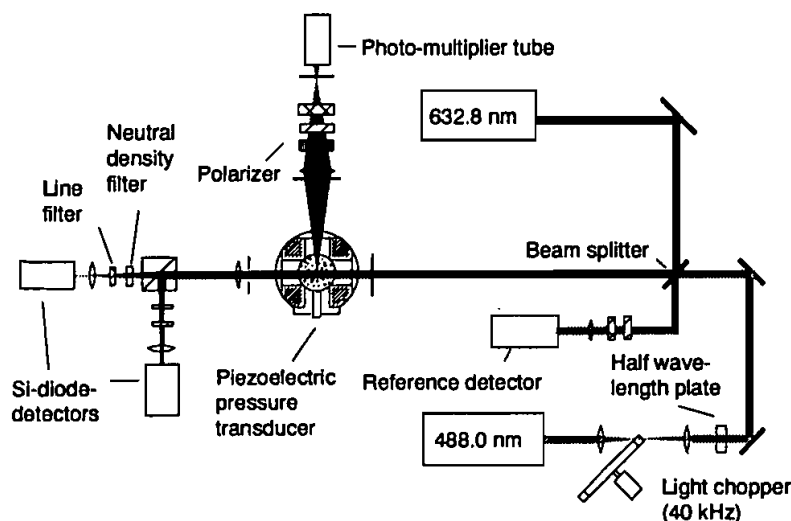


FIGURE 2 Optical setup for scattering and extinction measurements.

Extinction cross section  $C_{\text{ext}}$  and scattering function  $i_1$  are functions of the refractive index, the non-dimensional particle size  $\alpha = d\pi/\lambda$  and the scattering angle  $\Theta$ . Scattering measurements were carried out only for *n*-heptane shocks. To allow comparison with other fuels that have been investigated earlier induction periods and soot volume fraction were determined by extinction of a He-Ne laser at 632.8 nm. Corresponding to our results for particle diameters soot volume fraction was calculated assuming Rayleigh approximation.

$$f_v = \frac{\ln(I/I_0)\lambda}{6\pi l} \frac{1}{\text{Im}\left\{\frac{m^2-1}{m^2+2}\right\}} \quad (5)$$

## EXPERIMENTAL RESULTS AND DISCUSSION

For soot growth modeling soot particle size and number density are important quantities. They were calculated from the extinction and scattering cross section at 488 nm. A time profile for  $Q_{\text{VV}}$  and  $K_{\text{ABS}}$  is given in Figure 3 for a *n*-heptane shock at 25 bar and 1750 K,  $[C] = 7.89 \text{ mol/m}^3$ ,  $\phi = 5$ .

There is a slight absorption after the passage of the reflected shock ( $t \approx 0$ ) and then at 0.3 ms a steep rise is found that denotes the appearance of absorbing species. This does not necessarily mean soot particles but, especially in the absence of distinct scattering, large aromatic structures that are able to absorb at this wavelength. Similar observations have been made by Graham *et al.* (1975) in atmospheric pyrolysis of aromatic hydrocarbons. The increase of  $K_{\text{ABS}}$  is accompanied by a small peak of the scattering coefficient. However, experiments with longer

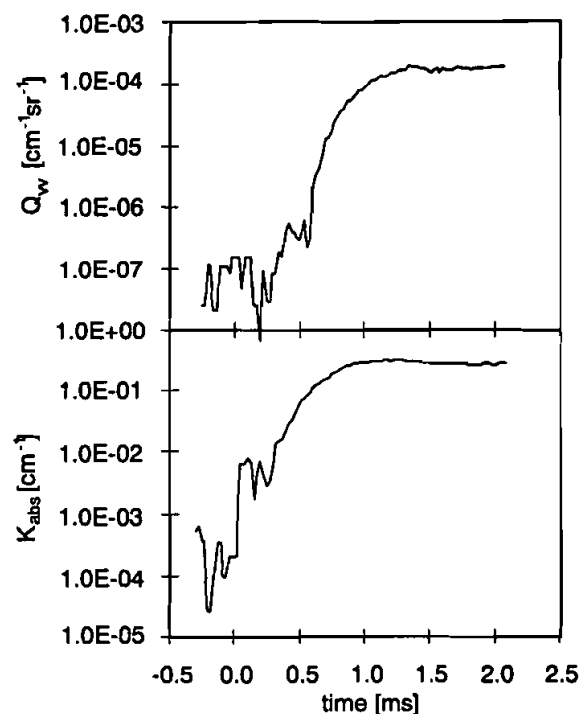


FIGURE 3 Scattering and absorption coefficients at 488 nm for a *n*-heptane shock at 25 bar and 1750 K,  $[C] = 7.89 \text{ mol/m}^3$ ,  $\phi = 5$ .

induction periods showed that this peak always appeared at ca. 0.3 ms after the reflected shock and is therefore not correlated with temperature. This phenomenon has been attributed to transparent particles by Lazzaro *et al.* (1994). As we also detected these signals in pure argon shocks with no measurable extinction we conclude that these signals are due to improper cleaning of the shock tube. The effect could be remarkably reduced if strong argon shocks were conducted in a row with cleaning in between. The appearance of solid soot particles is indicated by a strong increase of  $Q_{VV}$  at 0.5 ms.

Results for soot yield, defined as the carbon present as soot referred to the total carbon available, volumetric particle diameter and particle number density of the same run are presented in Figure 4. High soot mass growth rates lead to a steep increase in  $Y_s$  that diminishes with time, as will be discussed later in this paper. After a rapid growth that follows particle inception, the rise in particle diameter decreases with time to yield a volumetric diameter of 28 nm at the end of the observation time. The fast growth is accompanied by particle coagulation which reduces the number density quickly.

The measured final particle number density ( $\approx 10^{12}/\text{cm}^3$ ) was found to be significantly higher than at atmospheric flame conditions. Enhanced soot production at high pressures is therefore not a result of larger particles but accompanied by an

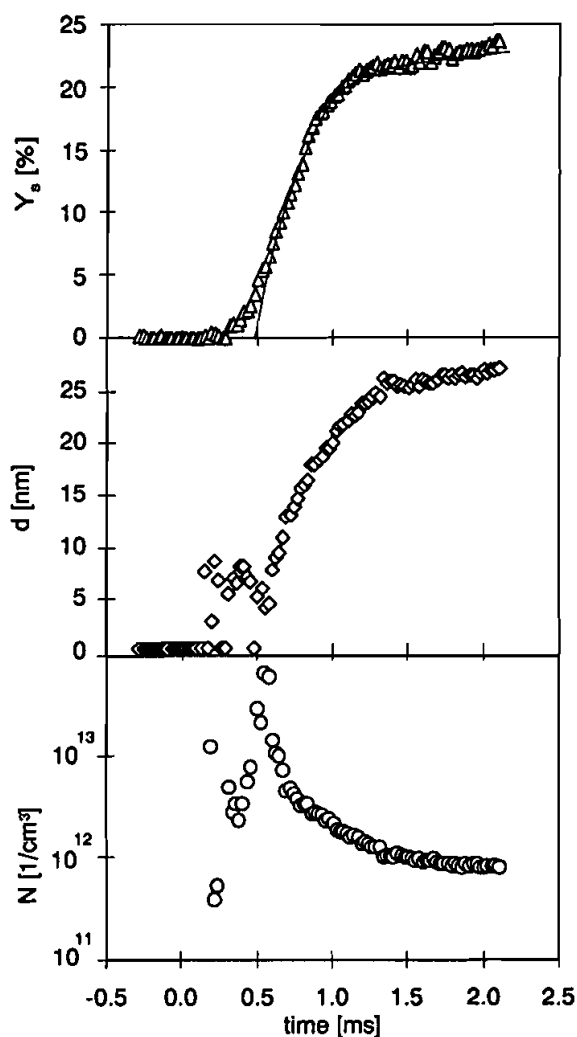


FIGURE 4 Soot yield, volumetric particle diameter and number density at 488 nm for a *n*-heptane shock at 25 bar and 1750 K,  $[C] = 7.89 \text{ mol/m}^3$ ,  $\phi = 5$ .

increase in number density. Reduced particles sizes can be attributed to lower coagulation coefficients in the transition regime between free molecular and continuum flow.

Measured particle sizes taken 1.5 ms after reflected shock arrival are shown for different pressure conditions in Figure 5. Largest particles are detected at temperatures around 1850 K with diameters decreasing toward lower and higher temperatures. The comparison at constant carbon concentration (25 bar, Ar = 98% to 100 bar, Ar = 99.5%) indicates that an increase of pressure at constant carbon density leads to smaller particle sizes, even though soot yield is clearly enhanced at higher pressures as will be shown later. According to the determined particle diameters, the

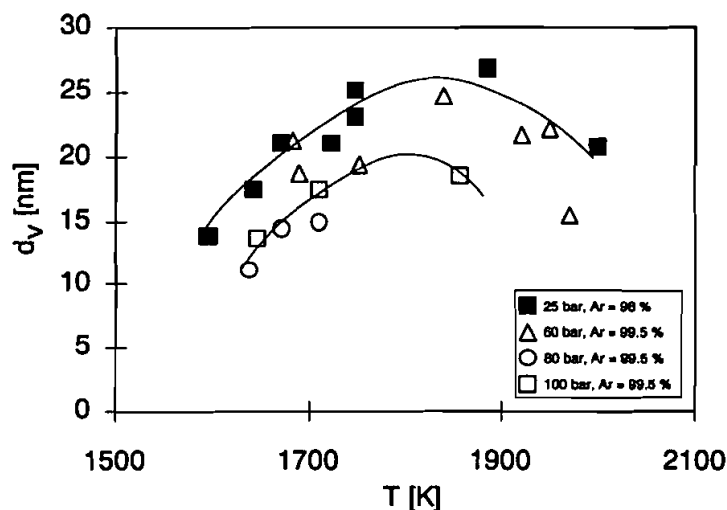


FIGURE 5 Particle diameters 1.5 ms after passage of the reflected shock determined by scattering-extinction at 488 nm for *n*-heptane ( $\phi = 5$ ). Values at 25 and 100 bar are measured for equal carbon concentrations of  $7.2 \text{ mol/m}^3$ .

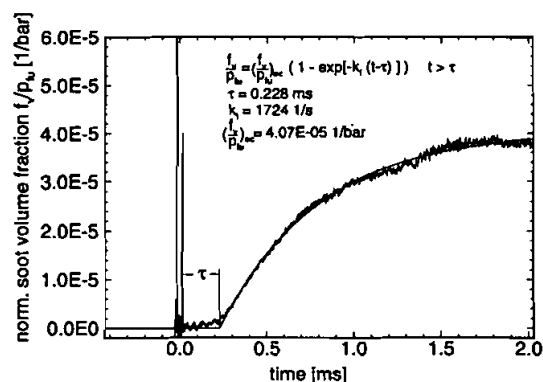


FIGURE 6 Time profile of shock tube soot growth behind reflected shock. Plotted is the soot volume fraction normalized by the fuel partial pressure  $f_v/p_{f,v}$  together with the model function for first order growth ( $\text{C}_3\text{H}_8$ ,  $\phi = 5$ ,  $\text{Ar} = 99\%$ ,  $p = 60 \text{ bar}$ ,  $T = 1940 \text{ K}$ ).

assumption of spheres which are small compared to the wavelength (Rayleigh approximation) has proved to be acceptable in our measurements.

A typical time profile of shock tube soot growth behind reflected shock is presented in Figure 6. Normalized soot volume fraction calculated from extinction at 632.8 nm for  $\text{C}_3\text{H}_8$  ( $\phi = 5$ ,  $\text{Ar} = 99\%$ ,  $p = 40 \text{ bar}$ ,  $T = 1940 \text{ K}$ ) is plotted versus measurement time. After the clearly visible passage of incident and reflected shock soot growth is delayed by a characteristic induction time  $\tau$ . During this period hydrocarbons are transformed into solid particles. The smooth onset of soot forma-

tion is followed by a period of maximum soot growth and finally tends towards a constant level. As induction time and soot growth depend on temperature, carbon concentration and pressure this plateau is not always reached during measurement time. In the region after maximum soot growth the behavior of soot volume fraction can be described by a first order growth law as suggested by Haynes and Wagner (1981).

$$\frac{df_v}{dt} = k_f(f_{v\infty} - f_v(t)) \quad (6)$$

Here,  $k_f$  is a first order growth constant and  $f_{v\infty}$  denotes the final soot volume fraction. Following this approach our measurements of soot volume fraction were evaluated in terms of this model to yield the characteristic values of  $f_{v\infty}$ ,  $k_f$  and  $\tau$  for each run as also demonstrated in Figure 6. Calculation of soot yield values was based on the final soot volume fraction and a soot density of 2 g/cm<sup>3</sup>.

There is no clear definition how to determine the induction period. In our experiments induction time was obtained as the period between the passage of the reflected shock and the intersection of the model function with the time axis. Other authors have used the first visible attenuation of the laser beam (Müller and Wittig 1991) or the intersection of the inflectional tangent with the time axis (Bauerle *et al.* 1994). A comparison of induction times achieved by these different definitions did not show a great impact on our results. Our measurements indicated that the induction period can be expressed by:

$$\frac{1}{\tau} = A[C]^n \exp\left(-\frac{E_{\text{ind}}}{RT}\right) \quad (7)$$

As already reported from earlier measurements (Müller and Wittig 1994), no influence of equivalence ratio or pressure on the induction period could be found. Therefore, increased pressure does not lead to a faster appearance of incipient soot particles.

The impact of  $[C]$  and temperature on induction time is demonstrated in Figure 7 for methane combustion. According to Arrhenius expression the logarithms of  $\tau$  are plotted versus  $1000/T$ .

Induction period is strongly reduced by higher temperatures and decreases with increased carbon atom concentration. Determined exponential factors for the impact of carbon concentration gave values between 0.35 and 0.46 for the fuels investigated (Tab. 1). The values in the table are based on  $\tau$  in [ms] and  $[C]$  in [mol/cm<sup>3</sup>]. For acetylene the carbon concentration range was too small to determine the exponential factor.

A comparison between different fuels is made in Figure 8. The determined induction periods for n-heptane are shown together with best fits for the other fuels under investigation. For comparability  $\tau$  for all hydrocarbons was normalized by  $[C]^{0.5}$ .

Longest induction times were achieved for methane, followed by propane and n-heptane. Shortest  $\tau$  is found for acetylene. The temperature dependence resulted in activation energies and pre-exponential factors that are also given in Table 1. Our results are in agreement with the generally accepted model of soot formation.



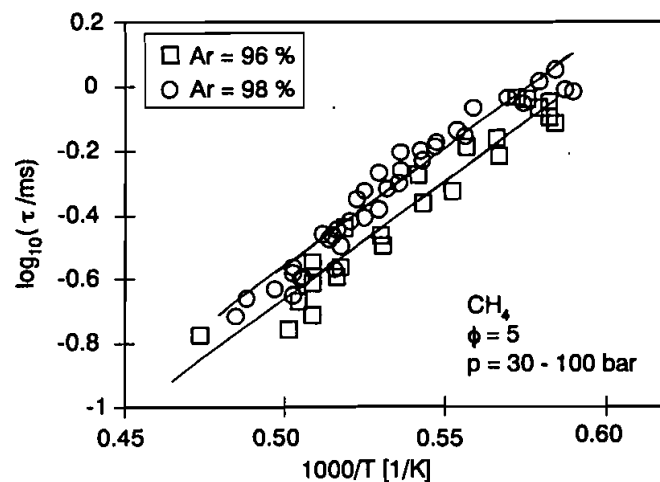


FIGURE 7 The influence of  $[C]$  on induction times is demonstrated for methane rich oxidation ( $\phi = 5$ ) at Ar-concentrations of 96% and 98%.

TABLE I

Induction periods for different aliphatic hydrocarbons

Fuel	A	n	$E_{ind}$ (kJ/mol)
methane	$1.64 \cdot 10^6$	0.35	145
propane	$7.31 \cdot 10^6$	0.42	149
<i>n</i> -heptane	$1.89 \cdot 10^7$	0.46	149
ethylene	$1.59 \cdot 10^7$	0.45	141
acetylene	$3.28 \cdot 10^5$		157

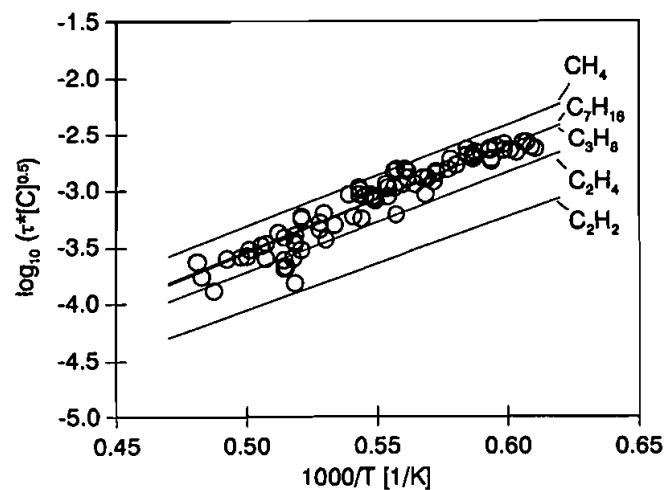


FIGURE 8 Induction periods for different hydrocarbons under investigation.

Acetylene, the main intermediate species before growth of aromatic structures, can form soot via direct route whereas alkenes and alkanes have first to be decomposed leading to longer induction times. First order rate constants  $k_f$  determined showed a weak dependence on temperature resulting in apparent activation energies between 40 and 100 kJ/mol if evaluated in Arrhenius form:

$$k_f = [C]^n \exp\left(\frac{-E_k}{RT}\right) \quad (8)$$

This considerably lower than in flames where typical values of 120–140 kJ/mol are found (Bockhorn *et al.* (1984). The influence of carbon concentration was found to be between  $n = 0.5$  and 1 depending on fuel.

Soot yield versus temperature is illustrated in Figure 9 for methane, *n*-heptane and propane soot formation at an equivalence ratio of 5 and a pressure of 40 bar. The temperature dependence gives the typical bell shaped curves that are well known from pyrolysis experiments (Graham *et al.* 1975), (Frenklach *et al.* 1984). They attribute this behaviour to a competition of ring formation and breakup. At temperatures higher than  $T_{\max}$  breakup dominates over formation and leads to reduced soot yields. Compared to pyrolysis results the temperature of maximum soot formation  $T_{\max}$  is shifted towards lower temperatures leading to a maximum at 1780 K for the three displayed fuels. This shift is a result of equivalence ratio on sooting behavior and has been analyzed by Müller and Wittig (1994) in more detail. The carbon concentrations were chosen to allow representation of different hydrocarbons by approximately one soot yield curve. Based on the carbon concentrations necessary to produce the same soot yield, Figure 9 indicates a similar sooting tendency for propane and *n*-heptane whereas methane shows a lower sooting propensity. In accordance with studies by Tanke (1994)  $T_{\max}$  for acetylene is found to be moved 150 K towards lower temperatures compared to *n*-heptane.

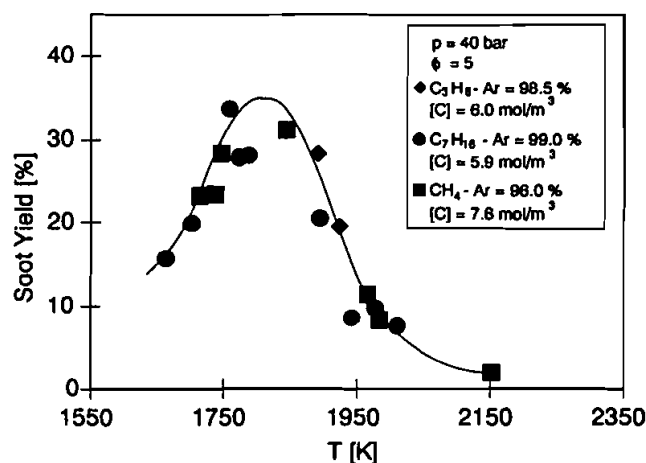


FIGURE 9 Soot yield ( $p = 40$  bar,  $\phi = 5$ ) as a function of temperature for different hydrocarbons under investigation.

The influence of pressure and carbon concentration on soot formation is demonstrated for *n*-heptane. Measurements were carried out for pressure ranging from 15–100 bar, carbon concentrations of 4.4 mol/m<sup>3</sup>, 5.8 mol/m<sup>3</sup> and 7.2 mol/m<sup>3</sup> and a temperature of 1600 to 2100 K. Previous results for soot formation of rich methane oxidation (Müller and Wittig 1991) showed an increasing effect of pressure on soot volume fraction and a dependence of  $f_v \sim p_{\text{fuel}}^2$  was found, where  $p_{\text{fuel}}$  denotes the fuel partial pressure.

Soot yields obtained for a constant carbon concentration of 5.8 mol/m<sup>3</sup> and pressures of 20, 40 and 80 bar are shown in Figure 10. The plot reveals that soot yield is substantially increased from 20 to 40 bar. However, there is a comparatively weak rise from 40 to 80 bar. Obviously, the pressure influence decreases with higher pressures. No influence of pressure on the temperature of maximum soot formation could be found. It is interesting to observe that the pressure effect is more pronounced in the region of maximum soot yield than at temperatures higher than 1950 K.

The effect of increased carbon concentration is demonstrated in Figure 11. Soot yield is plotted over temperature for a mixture of 99% Ar, 0.3125% C<sub>7</sub>H<sub>16</sub> and 0.6875% O<sub>2</sub>. Although pressure is only slightly varied a strong impact on soot yield is found. In accordance with the previous study for methane, carbon concentration effects soot formation more dominantly than pressure. The results do not exhibit a pronounced influence of carbon concentration of the temperature of maximum soot formation.

The impact of carbon concentration and pressure on soot yield is presented in more detail in Figure 12. Soot yield for different Ar-concentrations and pressures at constant temperature are compared. The temperature of 1800 K was chosen on the high temperature side of the soot yield curve, slightly higher than  $T_{\text{max}}$ . However, evaluation at other temperatures gave a similar tendency. The analysis allows the

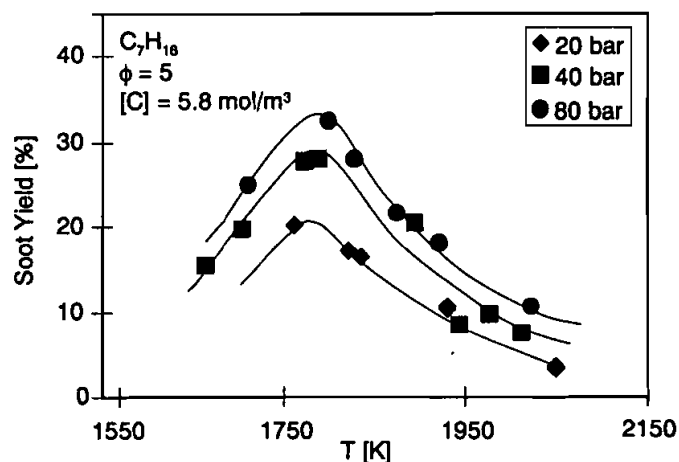


FIGURE 10 Influence of pressure on *n*-heptane soot yield demonstrated for pressures of 20, 40 and 80 bar at  $[C] = 5.8 \text{ mol/m}^3$ .

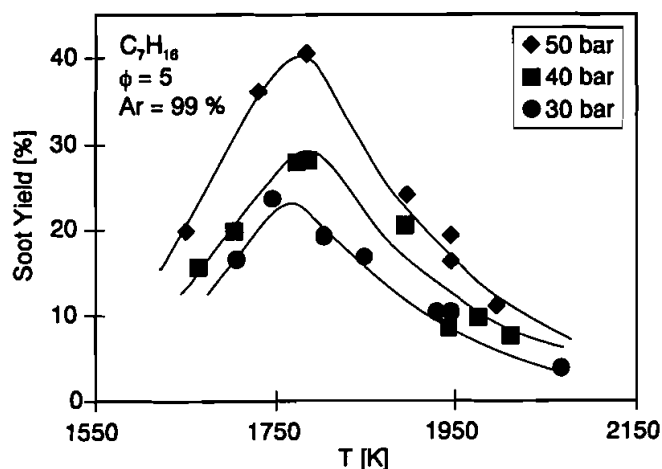


FIGURE 11 Soot yield over temperature at constant Ar-concentration of 99% and varied pressures of 30, 40 and 50 bar.

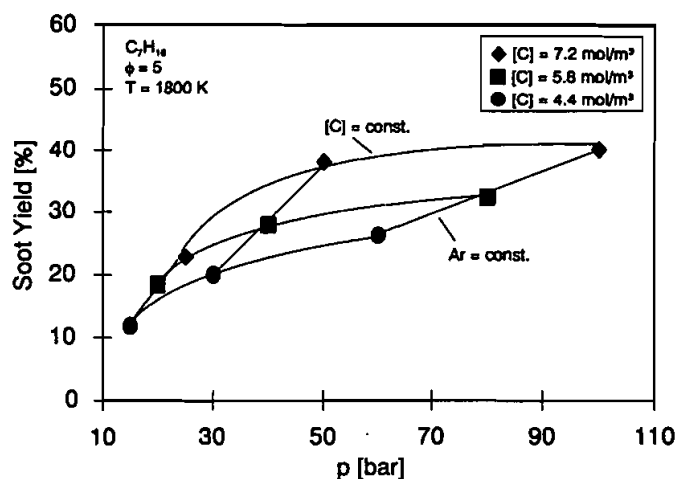


FIGURE 12 Influence of carbon atom concentration and pressure on *n*-heptane soot yield at 1800 K.

following conclusions to be drawn:

- Mixtures with constant Ar-concentration yield approximately a linear increase of soot yield with pressure.
- Pressure does have a strong influence at pressures lower than 30 bar that diminishes towards higher pressures. At the maximum investigated pressure of 100 bar the pressure effect has almost disappeared.
- Carbon concentration has a marked promoting influence on soot yield that can be described by  $f_v \sim [C]^3$  for pressures higher than 30 bar.

Pressure influence on pyrolysis of various hydrocarbons have been reported by Tanke (1994). No pressure dependence of soot yield in methane, n-hexane and acetylene pyrolysis was found. For methane the impact of carbon concentration resulted in  $f_p \sim [C]^3$  which is similar to our analysis for n-heptane. Comparing our results to the pyrolysis experiments for n-hexane cited above we have to observe a remarkable difference in the pressure dependence of soot formation. As n-hexane and n-heptane experience very similar molecular structures that should lead to equal sooting behaviour, the noted pressure effects could be the result of a change in mechanism between rich oxidation and pyrolysis.

## CONCLUSION

Scattering-extinction measurements have been performed under high pressure conditions in shock tube soot growth. Determined particle diameters were in the range below 30 nm, with particle sizes decreasing with pressure. Enhanced soot formation at high pressures is therefore accompanied by high particle number densities in range of  $N \approx 10^{12} - 10^{13}$  l/cm<sup>3</sup>. Investigation of the influence of carbon concentration resulted in a strong impact of  $f_p \sim [C]^3$  for n-heptane. Increased pressure did remarkably enhance soot yield at pressures lower than 30 bar. However, the promoting effect loses influence at higher pressures. The observed pressure effect for methane and n-heptane is in contradiction with results reported in literature where no pressure effect was found for soot formation from methane, n-hexane and acetylene pyrolysis and could therefore be result of a change in mechanism between pyrolysis and rich oxidation.

## ACKNOWLEDGEMENT

The authors gratefully acknowledge the support by the Deutsche Forschungsgemeinschaft within the Graduiertenkolleg "Energie- und Umwelttechnik".

## REFERENCES

- Bauerle, S., Karasevich, Y., Slavov, S., Tanke, D., Tappe, M., Thienel, T. and Wagner H. (1994). Soot Formation at Elevated Pressures and Carbon Concentrations in Hydrocarbon Pyrolysis. In *25th Symp. (Int.) on Combustion*.
- Bockhorn, H., Fetting, F., Heddrich, A. and Wannemacher G. (1984). Investigation of the Surface Growth of Soot in Flat Low Pressure Hydrocarbon Oxygen Flames. In *20th symp. (Int.) on Combustion*, pp.979.
- Böhm, H., Feldermann, C., Heidermann, T., Jander, H., Lüers, B. and Wagner H. (1992). Soot Formation in premixed C<sub>2</sub>H<sub>4</sub>-Air Flames for Pressure up to 100 bar. In *24th Symp. (Int.) on combustion*, pp. 991-998.
- Frenklach, M., Ramachandra, M. and Matula R. (1984). Soot formation in Shock Tube Oxidation of Hydrocarbons. In *20th Symp. (Int.) on combustion*, pp. 871.
- Graham, S., J. Homer, and J. Rosenfeld (1975). The Formation and Coagulation of Soot Aerosols Generated by the pyrolysis of Aromatic Hydrocarbons. In *Proc. Roy. Soc. Lond.*, Number A344, pp. 259.
- Haynes, B. and H. Wagner (1981). Soot Formation. *Prog. Energy Combustion Science*, 7, pp. 229.
- Kellerer, H., Bauer, H.-J. and Wittig S. (1995). Soot Formation from Rich Hydrocarbon Oxidation under Elevated Pressure Conditions. In *20th Int. Sump. On Shock Waves*.

- Lazzaro, M., Massoli, P. and d'Alessio J. (1994). Early Stages of Soot Formation in Shocked Ethylene studied by Laser Light Scattering/Extinction Measurements. In *Meeting of the French and the Italian Section of the Combustion Institute*.
- Lee, S. and Tien C. (1981). Optical Constants of Soot in Hydrocarbon Flames. In *18th Symp. (Int.) on Combustion*, pp. 1159.
- Müller, A. and Wittig S. (1991). Influence of temperature and pressure on soot formation in a shock tube under high pressure conditions. In *18th Int. Symp. on Shock Waves*.
- Müller, A. and Wittig S. (1994). Experimental study on the Influence of Pressure on Soot Formation. In H. Bockhorn (Ed.), *Soot Formation in Combustion: Mechanisms and Models of Soot Formation*, pp. 351–370. Springer.
- Parker, T., Foutter, R. and Rawlins W. (1989). Soot Initiation and Particle Growth in the Pyrolysis of Toluene at High Inert Gas Pressures. In *17th Symp. on Shock Tubes and Shock Waves*.
- Rudder, R. and Bach D. (1968). Rayleigh Scattering of Ruby-Laser Light by Neutral Gases. *J. of the Opt. Soc. of America* 58 (9), pp. 1260–1266.
- Tanke, D. (1994). *Soot Formation from Hydrocarbon Pyrolysis behind Shock Waves*. Dissertation, Universität Göttingen.
- Wagner, H. (1987). The Influence of Pressure on Soot Formation. In *AGARD Conference Proc. No. 422, Combustion and Fuels in Gas Turbine Engines*, pp. 24–1.
- Wittig, S., Müller, A. and Lester T. (1989). Time-resolved Soot Particle Growth in Shock Induced High Pressure Methane Combustion. In *17th symp. on Shock Tubes and Shock Waves*, pp. 468–473.